# Ring Polymer Molecular Dynamics Approach to Quantum Dissociative Chemisorption Rates

Liang Zhang, <sup>1</sup> Junxiang Zuo, <sup>1</sup> Yury V. Suleimanov, <sup>2</sup> and Hua Guo<sup>1,\*</sup>

<sup>1</sup>Department of Chemistry and Chemical Biology, University of New Mexico,

Albuquerque, New Mexico 87131

<sup>2</sup>American Association for the Advancement of Science, 1200 New York Ave NW,

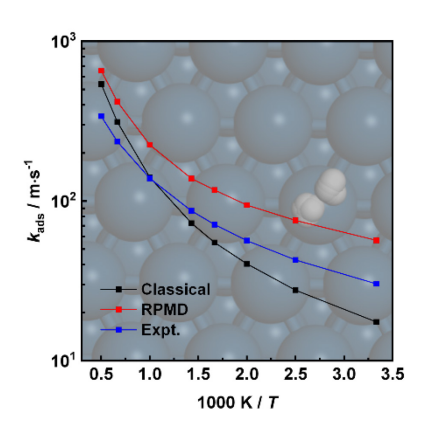
Washington, D.C. 20005

<sup>\*:</sup> corresponding author: hguo@unm.edu

### Abstract

A ring polymer molecular dynamics (RPMD) method is proposed for the calculation of dissociative chemisorption rate coefficient on surfaces. The RPMD rate theory is capable of handling quantum effects such as the zero-point energy and tunneling in the dissociative chemisorption, while relies on classical trajectories for the simulation. Applications to H<sub>2</sub> dissociative chemisorption are demonstrated. For the highly activated process on Ag(111), strong deviations from the Arrhenius behavior are found at low temperatures and attributed to tunneling. On Pt(111), where the dissociation has a barrierless pathway, the RPMD rate coefficient is found to agree with the experimentally derived thermal sticking coefficient within a factor of two over a large temperature range. Significant quantum effects are also found.

## TOC graphic



There is strong experimental evidence of nuclear quantum effects in reactions involving light atoms, in both the gas phase<sup>1</sup> and extended systems.<sup>2, 3</sup> Recently, the rates for recombinative desorption of H<sub>2</sub> on Pt surfaces were accurately measured for the first time and found to exhibit strong nuclear quantum effects even at the temperature of 1000 K.<sup>4</sup> These new experiments challenge theory to provide a first principles interpretation. In principle, the quantum rate coefficient can be computed by directly solving the Schrödinger equation. However, a quantum dynamical characterization of an elementary chemical reaction at the gas-solid interface is quite challenging,<sup>5-7</sup> due to the large number of surface degrees of freedom (DOFs). The conventional wave packet method based on an explicit solution of the time-dependent Schrödinger equation becomes impractical and there is strong desire to find a numerically efficient method to incorporate quantum effects in rate calculations for surface reactions.

An alternative way to rate calculations is the statistical approach such as the transition-state theory (TST), which, due to the ease of implementation, has become a popular method for bimolecular reactions in the gas phase.<sup>8</sup> The basic assumption is that the rate is determined by the thermal population of the activated complex, which once reached decays irreversibly to products.<sup>9, 10</sup> As a result, the rate coefficient can be obtained from the flux passing through a dividing surface between reactants and products, often placed near the reaction barrier. In a typical implementation,<sup>11</sup> the partition functions used in TST calculations are evaluated using the harmonic oscillator approximation. However, such approximations could drastically fail due to strong

anharmonicity in low-frequency modes, which are especially abundant in surface processes. When quantum tunneling is important, TST typically relies on a semiclassical treatment, 12 which might miss important multidimensional effects. Finally, TST does not rigorously take recrossing of the dividing surface into consideration, which can be quite important in some cases. 13 Dynamical corrections using classical trajectories have been suggested for high temperatures. 14

The ring polymer molecular dynamics (RPMD) approach proposed by Manolopoulos and coworkers<sup>15</sup> represents a promising alternative to TST in computing the rate coefficient.<sup>16-19</sup> The basic premise of RPMD is to take advantage of the isomorphism for statistical properties in a quantum and a fictitious classical system,<sup>20</sup> in which a quantum particle is replaced by a necklace of harmonically connected beads.<sup>15</sup> It is well suited to include quantum effects such as zero-point energy and tunneling.<sup>19</sup> In addition to the linear scaling law with respect to the number of particles in the system, the RPMD rate theory has a number of desirable properties. First, it is reduced to the classical limit when only one bead is used, which offers a convenient way to examine the impact of quantum effects.<sup>15</sup> Second, it is independent of the definition of the dividing surface,<sup>17</sup> which is very difficult to achieve in the conventional TST calculations.

The rate theory based on RPMD has been formulated by the *ad hoc* replacement of the classical Hamiltonian with the RPMD one. <sup>16, 17</sup> Its implementation to gas-phase bimolecular reactions <sup>18, 19, 21</sup> has been applied to many systems with great success. <sup>13</sup>

Surface reactions present additional challenges due to the large number of surface DOFs. So far, some applications of the RPMD approach have been reported for surface processes, <sup>22-27</sup> but none has been applied to chemical reactions where bond breaking and forming are present.

Recently, there is also significant interest in treating multidimensional tunneling using the quantum instanton theory (QI).<sup>28</sup> Applications of QI to dissociative chemisorption have been reported for several systems.<sup>29-31</sup> However, it has been shown for gas phase bimolecular reactions that RPMD outperforms QI in rate calculations.<sup>19,</sup>
<sup>32</sup> Furthermore, it is not clear how QI can be applied to a nominally barrierless process.

In this work, we present the adaptation of the RPMD rate theory to the dissociative chemisorption (DC) of H<sub>2</sub> using a rigid surface model. We investigated two special cases, one is the activated DC on Ag(111) and the other is the barrierless DC on Pt(111). Our results demonstrate reasonable agreement with the available experimental sticking rates in the latter case, and strong quantum effects in both cases.

We start with defining the rate equation for a DC process of a homonuclear diatom (e.g., H<sub>2</sub>) on an infinite surface:

$$H_2(g) \rightarrow 2H^*$$

where \* indicates the adsorbed state for the dissociated atomic fragments. The extension to a polyatomic system is trivial. The rate equation can be defined either in terms of the molecular concentration in the gas phase or by the coverage on the surface.

$$-\frac{d[H_2]}{dt} = \frac{1}{2} \frac{d[H^*]}{dt} = k(T)[H_2]. \tag{1}$$

Experimentally, it is more convenient to measure the coverage on the surface (with the unit of  $1/m^2$ ) so the rate coefficient k(T) is often given in the unit of m/s.<sup>4</sup>

Quantum mechanically, the rate coefficient can be written as,<sup>33</sup>

$$k(T) = \frac{1}{Q_r^{\square}(T)} c_{fs}^{\square}(t \to \infty), \tag{2}$$

where  $Q_r^{\square}(T)$  is the reactant quantum mechanical partition function per unit volume and  $c_{fs}^{\square}(t)$  the flux-side correlation function defined in the N-particle phase space  $\{p,q\}$ :

$$c_{fs}^{(1)}(t) = \frac{1}{(2\pi\hbar)^{3N}} \int d^{3N} \boldsymbol{p} \int d^{3N} \boldsymbol{q} \, e^{-\beta H(\boldsymbol{p},\boldsymbol{q})} \delta[\xi(\boldsymbol{q})] v_{\xi}(\boldsymbol{p},\boldsymbol{q}) h[\xi(\boldsymbol{q}_t)], \tag{3}$$

where the reciprocal temperature is given by  $\beta = 1/k_BT$ . The dividing surface is defined by  $\delta[\xi(q)]$  along the reaction coordinate  $\xi(q)$  and  $h[\xi(q_t)]$  is a Heaviside function, which counts the fraction of trajectories  $(p_t, q_t)$  passing through the dividing surface to the product side at time t. The initial velocity along the reaction coordinate  $\xi(q)$  is,

$$v_{\xi}(\boldsymbol{p},\boldsymbol{q}) = \sum_{i=1}^{N} \frac{\partial \xi(\boldsymbol{q})}{\partial q_{i}^{\square}} \frac{\boldsymbol{p}_{i}^{\square}}{m_{i}}.$$
(4)

With the ring polymer ansatz,<sup>15</sup> the Hamiltonian in Eq. (3) is replaced by the ring polymer counterpart:

$$H_n(\boldsymbol{p}, \boldsymbol{q}) =$$

$$\sum_{i=1}^{N} \sum_{j=1}^{n} \left( \frac{\left| \boldsymbol{p}_{i}^{(j)} \right|^{2}}{2m_{i}} + \frac{m_{i}}{2} \omega_{n}^{2} \left| \boldsymbol{q}_{i}^{(j)} - \boldsymbol{q}_{i}^{(j-1)} \right|^{2} \right) + \sum_{j=1}^{n} V\left( \boldsymbol{q}_{1}^{(j)}, \cdots, \boldsymbol{q}_{N}^{(j)} \right), \tag{5}$$

where each atom is replaced by a ring polymer consisting of n beads that are interconnected via harmonic springs with the spring frequency of  $\omega_n = \frac{1}{(\beta_n \hbar)}$ ,  $\beta_n = \frac{1}{nk_BT}$  is the n-bead reciprocal temperature,  $\boldsymbol{p}_i^{(j)}$  and  $\boldsymbol{q}_i^{(j)}$  are momentum and position vectors of the  $j^{th}$  bead of the  $i^{th}$  atom, respectively,  $m_i$  is the atomic mass of the  $i^{th}$  atom,

V is the potential energy surface (PES) of the N-atom system. The corresponding ring polymer rate theory assumes an analogous form to Eq. (3), with the ring polymer Hamiltonian in Eq. (5) and  $n \times 3N$  phase space. <sup>16, 17</sup>

For DC, two dividing surfaces are introduced in terms of the ring polymer centroid variables, analogous to the case of a bimolecular reaction in the gas phase. <sup>19</sup> The first dividing surface is located in the asymptotic reactant valley where the molecule is high above the surface,

$$s_0(\bar{\boldsymbol{q}}) = Z_{\infty} - Z,\tag{6}$$

where Z is the vertical distance between the center of mass (COM) of the dissociating molecule and the surface and  $Z_{\infty}$  is an adjustable parameter that is chosen to be sufficiently large to make the interaction between the molecule and the surface negligible. It can be readily shown (Appendix I) that the corresponding rate coefficient has the unit of m/s. The second dividing surface is located in the transition-state region and can be defined as,

$$s_1(\bar{q}) = (Z^{\ddagger} - Z) - (r^{\ddagger} - r),$$
 (7)

where r is the distance between two dissociation fragments,  $Z^{\ddagger}$  and  $r^{\ddagger}$  are the corresponding distances at the saddle point of the PES.

A suitable interpolating reaction coordinate  $\xi(\bar{q})$  that connects two dividing surfaces is given by,<sup>19</sup>

$$\xi(\bar{q}) = \frac{s_0(\bar{q})}{s_0(\bar{q}) - s_1(\bar{q})},\tag{8}$$

such that  $\xi \to 0$  as  $s_0 \to 0$  and  $\xi \to 1$  as  $s_1 \to 0$ . Here the overline notation  $\bar{q}$  indicates that we have taken the dividing surfaces  $s_0(\bar{q}) = 0$  and  $s_1(\bar{q}) = 0$  to be

functions of the centroid coordinate,

$$\bar{\boldsymbol{q}} = \frac{1}{n} \sum_{j=1}^{n} \boldsymbol{q}^{(j)} \tag{9}$$

of a ring polymer composed of *n* beads.

In practice, the RPMD rate coefficient is presented<sup>18, 19</sup> in the Bennett–Chandler factorization form, <sup>34, 35</sup>

$$k^{\text{RPMD}}(T) = k^{\text{QTST}}(T; \xi^{\ddagger}) \kappa (t \to t_p; \xi^{\ddagger}). \tag{10}$$

Here, the first term,  $k^{\text{QTST}}(T; \xi^{\ddagger})$ , is the centroid-density quantum transition state theory (QTST) rate coefficient<sup>17</sup> evaluated at the peak  $(\xi^{\ddagger})$  of the potential of mean force (PMF) along the reaction coordinate:

$$k^{\text{QTST}}(T) = \left(\frac{1}{2\pi\beta\mu_Z}\right)^{\frac{1}{2}} e^{-\beta[W(\xi^{\ddagger}) - W(0)]},\tag{11}$$

where  $\mu_Z$  is the molecular mass and  $W(\xi)$  is the PMF calculated by using umbrella integration:<sup>21, 36, 37</sup>

$$W(\xi^{\ddagger}) - W(0) = \int_{0}^{\xi^{\ddagger}} \sum_{i=1}^{N_{windows}} \left[ \frac{N_{i} P_{i}(\xi)}{\sum_{j=1}^{N_{windows}} N_{j} P_{j}(\xi)} \left( \frac{1}{\beta} \frac{\xi - \bar{\xi}_{i}}{(\sigma_{i})^{2}} - k_{i}(\xi - \xi_{i}) \right) \right] d\xi, (12)$$

with the probability distribution

$$P_i(\xi) = \frac{1}{\sigma_i \sqrt{2\pi}} exp \left[ -\frac{1}{2} \left( \frac{\xi - \bar{\xi}_i}{\sigma_i} \right)^2 \right]. \tag{13}$$

Here  $N_{windows}$  is the number of biasing windows placed along the reaction coordinate with a specific value  $\xi_i$  assigned to each window,  $N_i$  is the total number of steps sampled for window i,  $\bar{\xi}_i$  and  $\sigma_i^2$  are the mean value and the variance calculated for the ith window from the trajectory generated by the modified ring polymer Hamiltonian,

$$H_n^{\xi}(\mathbf{p}, \mathbf{q}) = H_n(\mathbf{p}, \mathbf{q}) - \frac{1}{\beta_n} \ln f_{\xi}(\bar{\mathbf{q}}) + 1/2 k_i (\xi(\bar{\mathbf{q}}) - \xi_i)^2, \tag{14}$$

where  $k_i$  is the force constant which defines the strength of the bias in window i and

$$f_{\xi}(\bar{\boldsymbol{q}}) = \left\{ \sum_{i=1}^{N} \frac{1}{2\pi\beta m_i} \left[ \frac{\partial \xi(\bar{\boldsymbol{q}})}{\partial \bar{\boldsymbol{q}}_i} \right]^2 \right\}^{\frac{1}{2}}.$$
 (15)

The second factor in Eq. (10),  $\kappa(t \to t_p; \xi^{\ddagger})$ , is the long-time limit of the timedependent ring polymer transmission coefficient. This is a dynamical correction to centroid density QTST that accounts for recrossing of the reaction coordinate  $\xi(\bar{q}) = \xi^{\ddagger}$  at  $t \to t_p$ ,  $t_p$  is a "plateau" time, and ensures that the resulting RPMD rate coefficient  $k_{\text{RPMD}}(T)$  will be independent of any choice of the dividing surface.<sup>19</sup> It is given by <sup>13</sup>

$$\kappa(t \to t_p; \xi^{\ddagger}) = \lim_{t \to t_p} \frac{\langle f_{\xi}(\bar{q})^{-1} v_{\xi}(p,q) h[\xi(\bar{q}_t) - \xi^{\ddagger}] \rangle_{\xi^{\ddagger}}}{\langle f_{\xi}(\bar{q})^{-1} v_{\xi}(p,q) h[v_{\xi}(\bar{p},\bar{q})] \rangle_{\xi^{\ddagger}}},$$
(16)

where the subscripts on the brackets indicate that the averages are over the constrained ensemble at  $\xi(\bar{q}) = \xi^{\ddagger}$  and the factor of  $f_{\xi}(\bar{q})^{-1}$  is a metric tensor correction for the effect of the constraint.<sup>38</sup>

In this work, we applied the RPMD rate theory for DC to two systems, one with a high barrier and the other with a null barrier. For simplicity, we have assumed a rigid surface approximation, which has been widely used in dynamics studies of H<sub>2</sub> DC thanks to the large mass disparity.<sup>5</sup> In addition, this constraint can be readily relaxed in RPMD calculations, thanks to the linear scaling laws.<sup>15</sup>

For the highly-activated  $H_2 + Ag(111)$  system, we employed the six-dimensional PES constructed by Jiang and  $Guo^{39}$  using the permutation invariant polynomial neural network (PIP-NN) approach.<sup>40, 41</sup> The lowest dissociation barrier for  $H_2$  on Ag(111) is at the bridge site, associated with a high and "late" barrier of 1.15 eV. A contour plot for the PES at this site is shown as a function of Z and r with the angular coordinates optimized in Fig. 1(a). Additional contour plots of the PES (Figs. S1 and S2) can be

found in Supporting Information (SI).

For the non-activated system, namely H<sub>2</sub> dissociation on Pt(111), there have been many previous theoretical calculations. 42-46 We choose to construct a new sixdimensional PIP-NN PES based on 1457 density functional theory (DFT) points generated by a trajectory-free active learning strategy. 47, 48 All DFT calculations were performed by the Vienna Ab-initio Simulation Package (VASP). 49, 50 The ionic coreelectron interactions were described by the projector-augmented wave (PAW) method,<sup>51</sup> and the Kohn-Sham valence electronic wave function was expanded in a plane-wave basis set with a kinetic energy cutoff at 400 eV. The surface of Pt(111) was modelled by a five-layer slab with a vacuum region of 15 Å in the vertical direction within a 2 × 2 (1/4 ML coverage) surface unit cell. The Brillouin zone was sampled using a  $9 \times 9 \times 1$   $\Gamma$ -centered k-points grid mesh. The exchange-correlation effects were represented within GGA using the PBEα-vdW-DF2 functional.<sup>46</sup> A total root mean squared error (RMSE) of 6.73 meV was obtained using the PIP-NN method. A twodimensional PES cut of the non-activated reaction path is shown in Fig. 1(b) for comparison, where the COM of H<sub>2</sub> is fixed on the top site and the angular coordinates optimized. Additional contour plots of the PES can be found in SI.

All calculations were performed using a home-made FORTRAN code in Cartesian atomic coordinates with the ring polymer Hamiltonian in Eq. (5), thus imposing no restriction on the overall rotational or translational motion of the system. For the calculation of the PMF, the reaction coordinate (-0.05 to 1.10) was divided by an equal size ( $d\xi = 0.01$ ) with the force constant of the biasing potential of 2.72 (T/K) eV using

the umbrella sampling technique as described above. In each sampling window, 60 constrained sampling trajectories of 100 ps were carried out, before which the system was equilibrated for 20 ps with the Andersen thermostat<sup>52</sup> for thermalization. After determining the PMF at each temperature, the transmission coefficient was computed. Specifically, a long (2 ns) parent trajectory was carried out with the ring-polymer centroid constrain at the peak of PMF via the SHAKE algorithm<sup>53</sup> after an initial equilibration period of 20 ps, constrained configurations were sampled once every 2 ps. For each of these configurations, 150 separate unconstrained ring polymer trajectories were spawned with different initial momenta sampled from a Boltzmann distribution. These trajectories for Ag(111) and Pt(111) were then propagated for 150 fs and 120 fs, respectively, which is long enough for the transmission coefficients to reach plateau values. The time step is selected to be 0.1 fs in all RPMD calculations. The classical rate coefficients were also calculated for comparison by setting the number of beads to one.

For H<sub>2</sub> DC on Ag(111), the thermal rate coefficients were calculated at a number of temperatures ranging from 300 to 1000 K. The convergence was tested with up to 32 beads, as shown in Fig. S3 at the representative temperature of 500 K. The parameter  $Z_{\infty}$  in Eq. (6) was set to 7 Å for all of the temperatures considered and the  $s_1$  dividing surface was placed at the barrier at the bridge site ( $\xi$  = 1.0 or Z=1.10 Å and r=1.27 Å). The converged RPMD PMFs along the reaction coordinate  $\xi$  are displayed in Fig. 2(a). As shown, the free-energy barrier increases from low to high temperatures due to the negative entropy change from reactants to the transition state. In Figs. 2(b) and 2(c),

the classical and RPMD PMFs are compared at two representative temperatures (500 and 1000 K), which shows the RPMD free-energy barrier is significantly lower than the classical counterpart. This trend becomes more pronounced at lower temperatures. At high temperatures, the difference can be attributed to the inclusion of ZPE in RPMD, while at low temperatures, both tunneling and ZPE contribute and it is difficult to distinguish the contributions from the two quantum effects.

The time-dependence of the converged RPMD transmission coefficient,  $\kappa(t; \xi^{\ddagger})$ , the dynamical factor, is shown in Fig. 3(a). Clearly, all the transmission coefficients reach plateau values after initial drops from one. The transmission coefficient increases slightly with decreasing temperature. This temperature dependence shows that the less available thermal energy at lower temperatures leads to less recrossing of the dividing surface.

The final RPMD rate coefficients are compared with the classical ones in Fig. 4(a) and listed in Table 1. It is clearly shown that the rate coefficients from converged RPMD simulations are larger than those from classical limit at all temperatures, owing to tunneling. It also shows that the difference in the rate coefficients between the classical and RPMD simulations increases with decreasing temperature, which is to be expected from the larger contribution of tunneling to the centroid-density QTST rate at the lower temperature as shown in Figs. 2(b) and 2(c). Unfortunately, there has been no experiment on this system and a comparison is thus not possible.

The calculation for the H<sub>2</sub> DC on Pt(111) follows the same protocol as Ag(111)

described above. In particular,  $Z_{\infty}$  was set to 7 Å and the  $s_1$  dividing surface was placed at the second submerged saddle point ( $\xi = 1.0$  or Z=1.55 Å and r=1.10 Å). The convergence was also tested with up to 32 beads, as shown in Fig. S4 at the representative temperature of 500 K. The converged RPMD PMFs are shown in Fig. 2(d) at a number of temperatures ranging from 300 to 2000 K. There is a free-energy barrier near the first submerged saddle point in the entrance channel. Despite the barrierless minimum energy path at the top site, the dissociation pathways at other surface sites all have non-negligible barriers, as shown in Fig. S2. The PMF thus represents an effective barrier for the impinging molecule. In the meantime, the second submerged saddle point shown in Fig. 1(b) does not lead to a free-energy barrier and has no impact on the kinetics. This is due to the fact that dissociation pathways in other surface sites possess no such a saddle point, as shown in Fig. S2. In addition, the freeenergy barrier on Pt(111) decreases with temperature and is much lower than Ag(111). Interestingly, there are still some small differences between the classical and quantum PMFs at two representative temperatures (500 and 2000 K), as shown in Fig. 2(e) and (f), suggesting the presence of quantum effects even for such lower barrier process. The quantum-classical difference in the barrier height becomes smaller at higher temperatures, as the system approaches the classical limit where the quantum effect is dominated by the ZPE.

As shown in Fig. 3(b), the transmission coefficients are smaller on Pt(111) than on Ag(111), indicating more recrossing, presumably due to the low effective barrier of the system. The recrossing is also more prominent at higher temperatures.

In Fig. 4(b) and Table 1, the calculated classical and quantum rate coefficients are compared with the experimental thermal sticking coefficients at several temperatures. The latter were derived in Ref.  $^4$  from previous experimental data. It can be seen from the figure that the experimental data do not follow the Arrhenius behavior, namely a straight line in the  $\log k - 1/T$  plot. This curvature of the temperature dependence is reproduced by both the classical and quantum results. The deviation from the Arrhenius behavior in the classical limit suggests that the curvature in the temperature dependence of the rate coefficient is not due to quantum effect. On the other hand, the difference between the classical and quantum rate coefficients is not large (a factor of three), and nearly independent with temperature. The RPMD rate coefficients are in reasonably good agreement with the experimental counterparts, within a factor of two, supporting the accuracy of the RPMD calculations.

The theory-experimental discrepancy, while small, might be attributable to a number of factors. First, the PES might contain errors due to the uncertainty associated with the functional. Second and perhaps more prominently, the rigid surface approximation used here might be inadequate. Although the mass of the H atoms is low compared with that of the metal, the fluctuation of the surface atoms might change the PES significantly to affect the kinetics. The impact of surface motion can in principle be included in RPMD calculations and we plan to explore this in future work.

In this work, the RPMD rate theory is extended to DC of gas phase molecules on surfaces and applied to two prototypical systems. The main advantage of the RPMD

approach is its ability to include quantum effects such as zero-point energy and tunneling, albeit approximately. In addition, it is numerically efficient for extended systems as the computation is based on classical trajectories. Although the numerical examples discussed in this work were based on rigid surface models, the inclusion of the surface atoms is straightforward.

The application of this RPMD rate theory to the highly activated H<sub>2</sub> DC on Ag(111) revealed strong nuclear quantum effects at low temperatures, resulting in a significant deviation from the Arrhenius behavior. This is attributed to tunneling of the impinging H<sub>2</sub> over the dissociative barrier. It is also demonstrated that the RPMD theory can be applied to systems where the dissociation minimum energy pathway involves no activation barrier, namely the DC of H<sub>2</sub> on Pt(111). Here, the calculated rate coefficient follows the same non-Arrhenius temperature dependence of the experimentally derived sticking coefficient within a factor of two. Moderate quantum effects are also seen. The favorable comparison with the experiment offers strong evidence for the reliability of the RPMD rate theory.

As discussed in Introduction, the RPMD rate theory has many advantages over other theoretical approaches including TST. It naturally avoids the harmonic oscillator approximation and is capable of handling soft modes. It treats the recrossing dynamics and the results are independent of the choice of the dividing surface, which is hard to define properly in a multidimensional space. Most importantly, it includes quantum effects such as tunneling and zero-point energy, thus ideally suited for studying nuclear

quantum effects. Finally, it scales linearly with the dimensionality of the system, which

is important for extended systems.

Finally, we emphasize that further applications of the RPMD to surface reactions

can be expected. For instance, the observed strong high-temperature quantum effects in

the recombinative desorption of H<sub>2</sub> and D<sub>2</sub> reported in the recent experiment<sup>4</sup> is

amenable to an RPMD characterization. Both Eley-Rideal and Langmuir-Hinshelwood

reactions can also be treated within the same framework. Such progress will

complement the recent advances in accurate rate measurements of elemental surface

reactions.54

Supporting information: Additional results on the PES and convergence.

Acknowledgments: This work was supported by the National Science Foundation

(CHE-1951328 and CHE-2306975 to H.G.) and the calculations were performed at the

Center for Advanced Research Computing (CARC) at UNM. We thank Florian Nitz,

Dima Borodin, and Alec Wodtke for providing experimentally derived thermal sticking

coefficients for H<sub>2</sub> on Pt(111), as reported in Ref. <sup>4</sup>, and for many stimulating

discussions. H.G. thanks the Alexander von Humboldt Foundation for a Humboldt

Research Award.

16

## Appendix I

It is well established that  $c_{fs}^{[i]}(t;s)$  is a real and odd function of t which is discontinuous at t=0 and has a positive limit as t tends to zero from above.<sup>33</sup> This leads to a well-defined TST approximation to the rate coefficient,

$$k^{QTST}(s) = \frac{1}{Q_r^{\square}(T)} c_{fs}^{\square}(t \to 0_+; s), \tag{I1}$$

where

$$c_{fs}^{(1)}(t \to 0_+; s) = \prod_{i=1}^{3N} \left(\frac{m_i}{2\pi\beta h^2}\right)^{1/2} \int d^{3N} \boldsymbol{q} \, e^{-\beta V(\boldsymbol{q})} \delta[s(\bar{\boldsymbol{q}})] f_s(\bar{\boldsymbol{q}}), \tag{I2}$$

with

$$f_s(\bar{\boldsymbol{q}}) = \left\{ \sum_{i=1}^N \frac{1}{2\pi\beta m_i} \left[ \frac{\partial s(\bar{\boldsymbol{q}})}{\partial \bar{\boldsymbol{q}}_i} \right]^2 \right\}^{\frac{1}{2}}.$$
 (I3)

When using the dividing surface  $s_0(\bar{q}) = Z_{\infty} - Z = 0$ , it becomes

$$f_{s_0}(\bar{\boldsymbol{q}}) = \left(\frac{1}{2\pi\beta\mu_Z}\right)^{\frac{1}{2}},\tag{I4}$$

and therefore

$$c_{fs}^{[]}(t \to 0_+; s_0) = \left(\frac{1}{2\pi\beta\mu_Z}\right)^{\frac{1}{2}} Q_r^{[]}(T),$$
 (I5)

where the reactant partition function is given as

$$Q_r^{\square}(T) = Q_{trans}^{\square}(T)Q_{int}^{\square}(T), \tag{16}$$

with

$$Q_{trans}^{\square}(T) = \left(\frac{\mu_Z}{2\pi\beta h^2}\right)^{1/2},\tag{I7}$$

and

$$Q_{int}^{\square}(T) = \left(\frac{\mu_r}{2\pi\beta\hbar^2}\right)^{3n/2} \int d^3\mathbf{r} \, e^{-\beta V_{int}(\mathbf{r})}.$$
 (I8)

Finally, substituting Eq. (I5) into Eq. (I1) gives

$$k^{QTST}(s_0) = \left(\frac{1}{2\pi\beta\mu_Z}\right)^{\frac{1}{2}},\tag{I9}$$

which is in the unit of m/s.

#### References:

- (1) Schatz, G. C. Tunneling in bimolecular collisions. *Chem. Rev.* **1987**, *87*, 81-89.
- (2) Meisner, J.; Kästner, J. Atom tunneling in chemistry. Angew. Chem. Int. Ed. 2016, 55, 2-16.
- (3) Markland, T. E.; Ceriotti, M. Nuclear quantum effects enter the mainstream. *Nat. Rev. Chem.* **2018**, *2*, 0109.
- (4) Borodin, D.; Hertl, N.; Park, G. B.; Schwarzer, M.; Fingerhut, J.; Wang, Y.; Zuo, J.; Nitz, F.; Skoulatakis, G.; Kandratsenka, A.; Auerbach, D. J.; Schwarzer, D.; Guo, H.; Kitsopoulos, T. N.; Wodtke, A. M. Quantum effects in thermal reaction rates at metal surfaces. *Science* **2022**, *377*, 394-398.
- (5) Kroes, G.-J. Six-dimensional quantum dynamics of dissociative chemisorption of H₂ on metal surfaces. *Prog. Surf. Sci.* **1999**, *60*, 1-85.
- (6) Jiang, B.; Yang, M.; Xie, D.; Guo, H. Quantum dynamics of polyatomic dissociative chemisorption on transition metal surfaces: Mode specificity and bond selectivity. *Chem. Soc. Rev.* **2016**, *45*, 3621-3640.
- (7) Shen, X.; Zhang, D. H. Recent advances in quantum dynamics studies of gas-surface reactions. *Adv. Chem. Phys.* **2018**, *163*, 77-116.
- (8) Truhlar, D. G.; Garrett, B. C.; Klippenstein, S. J. Current status of transition-state theory. *J. Phys. Chem.* **1996**, *100*, 12771-12800.
- (9) Eyring, H. The activated complex in chemical reactions. J. Chem. Phys. 1935, 3, 107-115.
- (10) Evans, M. G.; Polanyi, M. Some applications of the transition state method to the calculation of reaction velocities, especially in solution. *Trans. Faraday Soc.* **1935**, *31*, 875-894.
- (11) Steinfeld, J. I.; Francisco, J. S.; Hase, W. L. Chemical Kinetics and Dynamics, Prentice Hall, 1989.
- (12) Truhlar, D. G. Semiclassical Multidimensional Tunneling Calculations. In *Tunnelling in Molecules: Nuclear Quantum Effects from Bio to Physical Chemistry*, Kaestner, J., Kozuch, S. Eds.; RSC Publishing, 2021; pp 261-282.
- (13) Suleimanov, Y. V.; Aoiz, F. J.; Guo, H. Chemical reaction rate coefficients from ring polymer molecular dynamics: Theory and practical applications. *J. Phys. Chem. A* **2016**, *120*, 8488-8502.
- (14) Galparsoro, O.; Kaufmann, S.; Auerbach, D. J.; Kandratsenka, A.; Wodtke, A. M. First principles rates for surface chemistry employing exact transition state theory: application to recombinative desorption of hydrogen from Cu(111). *Phys. Chem. Chem. Phys.* **2020**, *22*, 17532-17539.
- (15) Craig, I. R.; Manolopoulos, D. E. Quantum statistics and classical mechanics: Real time correlation frunction from ring polymer molecular dynamics. *J. Chem. Phys.* **2004**, *121*, 3368-3373.
- (16) Craig, I. R.; Manolopoulos, D. E. Chemical reaction rates from ring polymer molecular dynamics. *J. Chem. Phys.* **2005**, *122*, 084106.
- (17) Craig, I. R.; Manolopoulos, D. E. A refined ring polymer molecular dynamics theory of chemical reaction rates. *J. Chem. Phys.* **2005**, *123*, 034102.
- (18) Collepardo-Guevara, R.; Suleimanov, Y. V.; Manolopoulos, D. E. Bimolecular reaction rates from ring polymer molecular dynamics. *J. Chem. Phys.* **2009**, *130*, 174713.
- (19) Suleimanov, Y. V.; Collepardo-Guevara, R.; Manolopoulos, D. E. Bimolecular reaction rates from ring polymer molecular dynamics: Application to H + CH<sub>4</sub>  $\rightarrow$  H<sub>2</sub> + CH<sub>3</sub>. *J. Chem. Phys.* **2011**, *134*, 044131.
- (20) Chandler, D.; Wolynes, P. G. Exploiting the isomorphism between quantum theory and classical statistical mechanics of polyatomic fluids. *J. Chem. Phys.* **1981**, *74*, 4078-4095.
- (21) Suleimanov, Y. V.; Allen, J. W.; Green, W. H. RPMDrate: bimolecular chemical reaction rates

- from ring polymer molecular dynamics. Comput. Phys. Comm. 2013, 184, 833-840.
- (22) Suleimanov, Y. V. Surface diffusion of hydrogen on Ni(100) from ring polymer molecular dynamics. *J. Phys. Chem. C* **2012**, *116*, 11141-11153.
- (23) Fang, W.; Richardson, J. O.; Chen, J.; Li, X.-Z.; Michaelides, A. Simultaneous deep tunneling and classical hopping for hydrogen diffusion on metals. *Phys. Rev. Lett.* **2017**, *119*, 126001.
- (24) Jiang, H.; Kammler, M.; Ding, F.; Dorenkamp, Y.; Manby, F. R.; Wodtke, A. M.; Miller, T. F.; Kandratsenka, A.; Bünermann, O. Imaging covalent bond formation by H atom scattering from graphene. *Science* **2019**, *364*, 379-382.
- (25) Liu, Q.; Zhang, L.; Li, Y.; Jiang, B. Ring polymer molecular dynamics in gas–surface reactions: Inclusion of quantum effects made simple. *J. Phys. Chem. Lett.* **2019**, *10*, 7475-7481.
- (26) Gu, K.; Li, C.; Jiang, B.; Lin, S.; Guo, H. Short- and long-time dynamics of hydrogen spillover from a single atom platinum active site to the Cu(111) host surface. *J. Phys. Chem. C* **2022**, *126*, 17093-17101.
- (27) Li, C.; Li, Y.; Jiang, B. First-principles surface reaction rates by ring polymer molecular dynamics and neural network potential: role of anharmonicity and lattice motion. *Chem. Sci.* **2023**, *14*, 5087-5098.
- (28) Miller, W. H.; Zhao, Y.; Ceotto, M.; Yang, S. Quantum instanton approximation for thermal rate constants of chemical reactions. *J. Chem. Phys.* **2003**, *119*, 1329-1342.
- (29) Wang, W.; Zhao, Y. Effect of lattice motion on dissociation and recombination rates of H<sub>2</sub> on Ni(100) surface. *J. Phys. Chem. C* **2013**, *117*, 19010-19019.
- (30) Wang, W.; Zhao, Y. The dissociation and recombination rates of CH<sub>4</sub> through the Ni(111) surface: The effect of lattice motion. *J. Chem. Phys.* **2017**, *147*, 044703.
- (31) Wang, W. Physisorbed state regulates the dissociation mechanism of H<sub>2</sub>O on Ni(100). *J. Phys. Chem. A* **2020**, *124*, 8724-8732.
- (32) Pérez de Tudela, R.; Suleimanov, Y. V.; Richardson, J. O.; Sáez Rábanos, V.; Green, W. H.; Aoiz,
- F. J. Stress test for quantum dynamics approximations: Deep tunneling in the muonium exchange reaction D + HMu  $\rightarrow$  DMu + H. *J. Phys. Chem. Lett.* **2014**, *5*, 4219-4224.
- (33) Miller, W. H.; Schwartz, S. D.; Tromp, J. W. Quantum mechanical rate constants for bimolecular reactions. *J. Chem. Phys.* **1983**, *79*, 4889-4899.
- (34) Bennett, C. H. Molecular dynamics and transition state theory: the simulation of infrequent events. In *Algorithms for Chemical Computations, ACS Symposium Series*, Christofferson, R. E. Ed.; Vol. 46; ACS, 1977.
- (35) Chandler, D. Statistical mechanics of isomerization dynamics in liquids and the transition state approximation. *J. Chem. Phys.* **1978**, *68*, 2959-2970.
- (36) Kästner, J.; Thiel, W. Bridging the gas between thermodynamic integration and umbrella sampling provides a novel analysis method: "umbrella integration". *J. Chem. Phys.* **2005**, *123*, 144104.
- (37) Kästner, J.; Thiel, W. Analysis of the statistical error in umbrella sampling simulations by umbrella integration. *J. Chem. Phys.* **2006**, *124*, 234106.
- (38) Frenkel, D.; Smit, B. *Understanding Molecular Simulation, Second Edition: From Algorithms to Applications* Academic Press, 2002.
- (39) Jiang, B.; Guo, H. Six-dimensional quantum dynamics for dissociative chemisorption of  $H_2$  and  $D_2$  on Ag(111) on a permutation invariant potential energy surface. *Phys. Chem. Chem. Phys.* **2014**, *16*, 24704-24715.

- (40) Jiang, B.; Guo, H. Permutation invariant polynomial neural network approach to fitting potential energy surfaces. *J. Chem. Phys.* **2013**, *139*, 054112.
- (41) Jiang, B.; Guo, H. Permutation invariant polynomial neural network approach to fitting potential energy surfaces. III. Molecule-surface interactions. *J. Chem. Phys.* **2014**, *141*, 034109.
- (42) Olsen, R. A.; Kroes, G. J.; Baerends, E. J. Atomic and molecular hydrogen interacting with Pt(111). *J. Chem. Phys.* **1999**, *111*, 11155-11163.
- (43) Pijper, E.; Kroes, G. J.; Olsen, R. A.; Baerends, E. J. Reactive and diffractive scattering of H₂ from Pt(111) studied using a six-dimensional wave packet method. *J. Chem. Phys.* **2002**, *117*, 5885-5898.
- (44) Pijper, E.; Kroes, G.-J.; Olsen, R. A.; Baerends, E. J. The effect of corrugation on the quantum dynamics of dissociative and diffractive scattering of H<sub>2</sub> from Pt(111). *J. Chem. Phys.* **2000**, *113*, 8300-8312.
- (45) Crespos, C.; Collins, M. A.; Pijper, E.; Kroes, G.-J. Application of the modified Shepard interpolation method to the determination of the potential energy surface for a molecule–surface reaction:  $H_2$  + Pt(111). *J. Chem. Phys.* **2004**, *120*, 2392-2404.
- (46) Ghassemi, N. E.; Wijzenbroek, M.; Somers, M. F.; Kroes, G.-J. Chemically accurate simulation of dissociative chemisorption of D<sub>2</sub> on Pt(111). *Chem. Phys. Lett.* **2017**, *683*, 329-335.
- (47) Lin, Q.; Zhang, Y.; Zhao, B.; Jiang, B. Automatically growing global reactive neural network potential energy surfaces: A trajectory-free active learning strategy. *J. Chem. Phys.* **2020**, *152*, 154104.
- (48) Lin, Q.; Zhang, L.; Zhang, Y.; Jiang, B. Searching configurations in uncertainty space: Active learning of high-dimensional neural network reactive potentials. *J. Chem. Theo. Comput.* **2021**, *17*, 2691-2701.
- (49) Kresse, G.; Furthmuller, J. Efficient iterative schemes for ab initio total-energy calculations using plane wave basis set. *Phys. Rev. B* **1996**, *54*, 11169-11186.
- (50) Kresse, G.; Furthmuller, J. Efficiency of ab initio total energy calculations for metals and semiconductors using plane wave basis set. *Comp. Mater. Sci.* **1996**, *6*, 15-50.
- (51) Blöchl, P. E. Projector augmented-wave method. Phys. Rev. B 1994, 50, 17953-17979.
- (52) Andersen, H. C. Molecular dynamics simulations at constant pressure and/or temperature. *J. Chem. Phys.* **1980**, *72*, 2384-2393.
- (53) Ryckaert, J. P.; Ciccotti, G.; Berendsen, H. J. Numerical integration of the cartesian equations of motion of a system with constraints: molecular dynamics of n-alkanes. *J. Comput. Phys.* **1977**, *23*, 327-341.
- (54) Park, G. B.; Kitsopoulos, T. N.; Borodin, D.; Golibrzuch, K.; Neugebohren, J.; Auerbach, D. J.; Campbell, C. T.; Wodtke, A. M. The kinetics of elementary thermal reactions in heterogeneous catalysis. *Nat. Rev. Chem.* **2019**, *3*, 723-732.

Table 1 Summary of centroid-density QTST rate coefficients, transmission coefficients and RPMD rate coefficients for  $H_2$  DC on Ag(111) and Pt(111) in the temperature interval between 300 and 1000 K. The centroid-density QTST and RPMD rate coefficients are given in m/s and the numbers in parentheses denote powers of 10.

	T(K)	$N_{ m bead}$	$k_{ m QTST}$	κ	$k_{ m RPMD}$
Ag(111)	300	32	4.30(-16)	0.905	3.89(-16)
	400	32	7.56(-12)	0.899	6.80(-12)
	500	32	3.47(-09)	0.882	3.06(-09)
	600	32	2.51(-07)	0.875	2.20(-07)
	700	16	5.67(-06)	0.865	4.90(-06)
	1000	16	2.05(-03)	0.845	1.73(-03)
Pt(111)	300	32	9.71(+01)	0.584	5.67(+01)
	400	32	1.34(+02)	0.565	7.57(+01)
	500	32	1.73(+02)	0.546	9.45(+01)
	600	32	2.17(+02)	0.540	1.17(+02)
	700	16	2.59(+02)	0.534	1.38(+02)
	1000	16	4.05(+02)	0.555	2.25(+02)
	1500	8	7.09(+02)	0.589	4.18(+02)
	2000	8	1.07(+03)	0.612	6.55(+02)

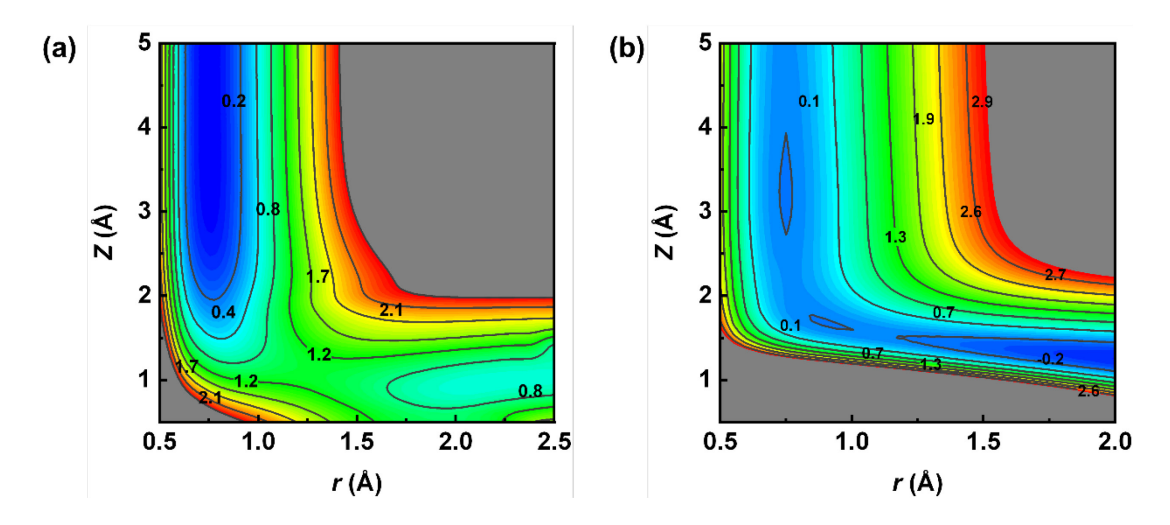


Fig. 1. Two-dimensional contour plots with the COM of  $H_2$  fixed on the bridge site of Ag(111) (a) and the top site on Pt(111) (b), with the angular coordinates optimized. There is a substantial barrier height of 1.15 eV for  $H_2$  dissociation on Ag(111), while  $H_2$  dissociation on Pt(111) has no intrinsic barrier, but contains two submerged saddle points.

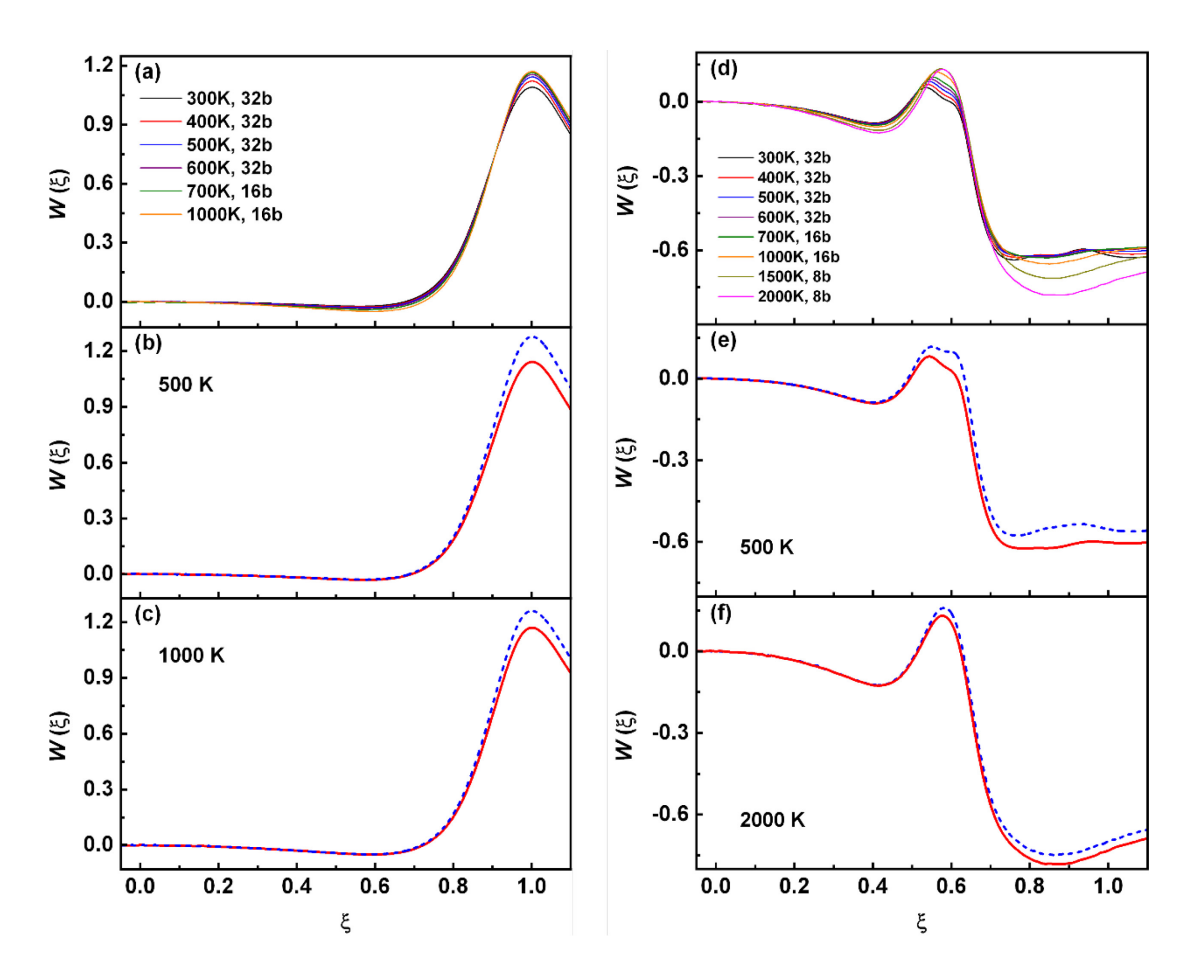


Fig. 2. Converged RPMD PMFs ( $W(\zeta)$  in eV, with the number of beads marked) for the H<sub>2</sub> DC (a and d) and comparison of the classical (dashed blue line) and RPMD (solid red line) PMFs at two temperatures (b, c and e, f). The left and right panels are for Ag(111) and on Pt(111), respectively.

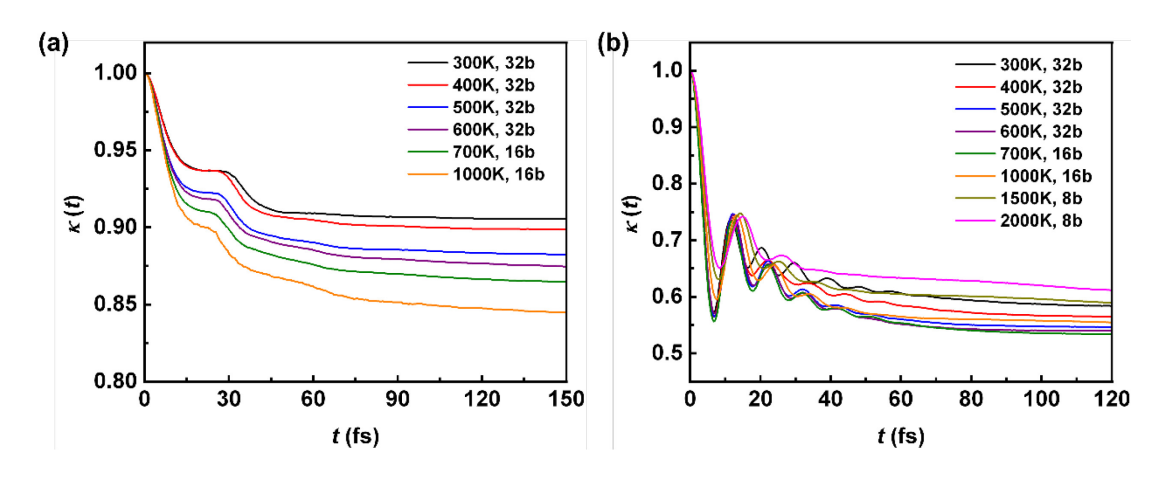


Fig. 3. Converged RPMD transmission coefficients (with the number of beads marked) for the  $H_2$  DC. The left and right panels are for Ag(111) and on Pt(111), respectively.

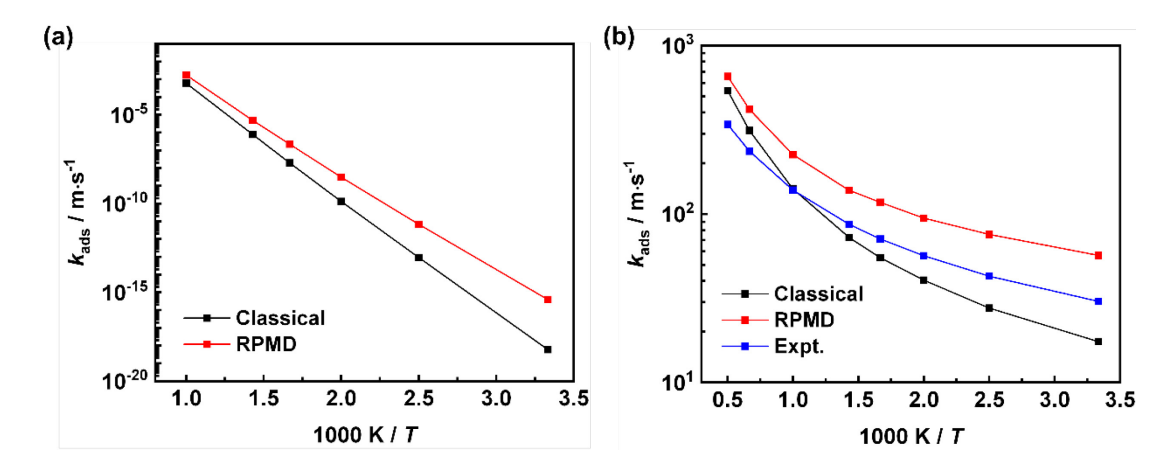


Fig. 4. Arrhenius plots of classical, RPMD and available experimental rate coefficients for the  $H_2$  DC. The left and right panels are for Ag(111) and on Pt(111), respectively.